HHS Public Access

Author manuscript

Neuroimage. Author manuscript; available in PMC 2023 February 06.

Published in final edited form as:

Neuroimage. 2022 December 01; 264: 119740. doi:10.1016/j.neuroimage.2022.119740.

Neurometabolic timecourse of healthy aging

Tao Gong[a,b,#], **Steve C.N. Hui**[c,d,#], **Helge J. Zöllner**[c,d], **Mark Britton**[e,f,g], **Yulu Song**[c,d], **Yufan Chen**[b], **Aaron T. Gudmundson**[h], **Kathleen E. Hupfeld**[c,d], **Christopher W. Davies-Jenkins**[c,d], **Saipavitra Murali-Manohar**[c,d], **Eric C. Porges**[e,f,g], **Georg Oeltzschner**[c,d], **Weibo Chen**[i], **Guangbin Wang**[a,b,*], **Richard A.E. Edden**[c,d]

[a]Departments of Radiology, Shandong Provincial Hospital Affiliated to Shandong First Medical University, Jinan, Shandong 250021, China

[b]Departments of Radiology, Shandong Provincial Hospital, Shandong University, Jinan, Shandong 250021, China

[c]The Russell H. Morgan Department of Radiology and Radiological Science, Johns Hopkins University School of Medicine, Baltimore, MD, United States of America

[d]F.M. Kirby Research Center for Functional Brain Imaging, Kennedy Krieger Institute, Baltimore, MD, United States of America

[e]Center for Cognitive Aging and Memory, University of Florida, Gainesville, FL, United States of America

[f]McKnight Brain Research Foundation, University of Florida, FL, United States of America

[g]Department of Clinical and Health Psychology, University of Florida, Gainesville, FL, United States of America

[h]Department of Neurobiology and Behavior, University of California, Irvine, CA, United States of America

[*]Corresponding author. wgb7932596@hotmail.com (G. Wang).
[#]Tao Gong and Steve C. N. Hui contributed equally to this work.

Data and code availability statements

All in vivo MR spectroscopy data were collected prospectively using 3T MRI. They will be available on the NITRC portal in the "Macromolecular MRS" project repository (https://www.nitrc.org/projects/MacromolecularMRS/). Data analysis was performed using the Osprey (https://github.com/schorschinho/osprey) software and MAT-LAB (R2020b, MathWorks, Natick, USA). Statistical analyses were done using R (RStudio: Integrated Development for R. RStudio, PBC, Boston, MA). All functions and packages are freely available on MATHWORKS and GITHUB. All the code and Fig.s are freely available on OSF (https://osf.io/upnkd/).

Declaration of Competing Interest

All authors declare no conflicts of interest.

Credit authorship contribution statement

Tao Gong: Writing – original draft, Resources, Investigation, Funding acquisition. **Steve C.N. Hui:** Writing – original draft, Methodology. **Helge J. Zöllner:** Data curation, Formal analysis. **Mark Britton:** Methodology, Validation, Formal analysis. **Yulu Song:** Data curation. **Yufan Chen:** Resources, Investigation. **Aaron T. Gudmundson:** Data curation, Formal analysis. **Kathleen E. Hupfeld:** Visualization, Writing – review & editing. **Christopher W. Davies-Jenkins:** Validation. **Saipavitra Murali-Manohar:** Writing – review & editing. **Eric C. Porges:** Validation, Formal analysis. **Georg Oeltzschner:** Software, Methodology. **Weibo Chen:** Software, Resources. **Guangbin Wang:** Project administration, Investigation, Writing – review & editing. **Richard A.E. Edden:** Conceptualization, Supervision, Project administration, Writing – review & editing, Funding acquisition.

Supplementary materials

Supplementary material associated with this article can be found, in the online version, at doi:10.1016/j.neuroimage.2022.119740.

[i]Philips Healthcare, Shanghai, China

Abstract

Purpose: The neurometabolic timecourse of healthy aging is not well-established, in part due to diversity of quantification methodology. In this study, a large structured cross-sectional cohort of male and female subjects throughout adulthood was recruited to investigate neurometabolic changes as a function of age, using consensus-recommended magnetic resonance spectroscopy quantification methods.

Methods: 102 healthy volunteers, with approximately equal numbers of male and female participants in each decade of age from the 20s, 30s, 40s, 50s, and 60s, were recruited with IRB approval. MR spectroscopic data were acquired on a 3T MRI scanner. Metabolite spectra were acquired using PRESS localization (TE=30 ms; 96 transients) in the centrum semiovale (CSO) and posterior cingulate cortex (PCC). Water-suppressed spectra were modeled using the Osprey algorithm, employing a basis set of 18 simulated metabolite basis functions and a cohort-mean measured macromolecular spectrum. Pearson correlations were conducted to assess relationships between metabolite concentrations and age for each voxel; Spearman correlations were conducted where metabolite distributions were non-normal. Paired t-tests were run to determine whether metabolite concentrations differed between the PCC and CSO. Finally, robust linear regressions were conducted to assess both age and sex as predictors of metabolite concentrations in the PCC and CSO and separately, to assess age, signal-noise ratio, and full width half maximum (FWHM) linewidth as predictors of metabolite concentrations.

Results: Data from four voxels were excluded (2 ethanol; 2 unacceptably large lipid signal). Statistically-significant age*metabolite Pearson correlations were observed for tCho ($r(98)=0.33$, $p<0.001$), tCr ($r(98)=0.60$, $p<0.001$), and mI ($r(98)=0.32$, $p=0.001$) in the CSO and for NAAG ($r(98)=0.26$, $p=0.008$), tCho($r(98)=0.33$, $p<0.001$), tCr ($r(98)=0.39$, $p<0.001$), and Gln ($r(98)=0.21$, $p=0.034$) in the PCC. Spearman correlations for non-normal variables revealed a statistically significant correlation between sI and age in the CSO ($r(86)=0.26$, $p=0.013$). No significant correlations were seen between age and tNAA, NAA, Glx, Glu, GSH, PE, Lac, or Asp in either region (all $p>0.20$). Age associations for tCho, tCr, mI and sI in the CSO and for NAAG, tCho, and tCr in the PCC remained when controlling for sex in robust regressions. CSO NAAG and Asp, as well as PCC tNAA, sI, and Lac were higher in women; PCC Gln was higher in men. When including an age*sex interaction term in robust regression models, a significant age*sex interaction was seen for tCho ($F(1,96)=11.53$, $p=0.001$) and GSH ($F(1,96)=7.15$, $p=0.009$) in the CSO and tCho ($F(1,96)=9.17$, $p=0.003$), tCr ($F(1,96)=9.59$, $p=0.003$), mI ($F(1,96)=6.48$, $p=0.012$), and Lac ($F(1,78)=6.50$, $p=0.016$) in the PCC. In all significant interactions, metabolite levels increased with age in females, but not males. There was a significant positive correlation between linewidth and age. Age relationships with tCho, tCr, and mI in the CSO and tCho, tCr, mI, and sI in the PCC were significant after controlling for linewidth and FWHM in robust regressions.

Conclusion: The primary (correlation) results indicated age relationships for tCho, tCr, mI, and sI in the CSO and for NAAG, tCho, tCr, and Gln in the PCC, while no age correlations were found for tNAA, NAA, Glx, Glu, GSH, PE, Lac, or Asp in either region. Our results provide a normative foundation for future work investigating the neurometabolic time course of healthy aging using MRS.

Keywords

magnetic resonance spectroscopy; neurometabolite; PRESS; healthy aging

1. Introduction

With the global population aging and the prevalence of Alzheimer's disease increasing (Langa et al., 2004), the study of the biochemical mechanisms of healthy and pathological aging is a major research priority. While cell-level neuroscience offers maximum scientific control and analytic precision, the need to link neurometabolic changes in the brain to changes in cognition, especially with a view to developing neuroprotective interventions, demands *in vivo* imaging methods. In-vivo magnetic resonance spectroscopy (MRS) of the brain can potentially bridge between cellular neuroscience and in vivo imaging of physical properties of tissue water by measuring the concentration of endogenous metabolites, particularly those associated with neurotransmission, energy metabolism and oxidative stress defense.

Major neurometabolites quantifiable by MRS include the neuronal marker N-acetyl aspartate (NAA) (Landim et al., 2016), as well as glutamate (Glu) (Cheng et al., 2021), the principal excitatory neurotransmitter. Glutamine (Gln) is an MRS-detectable precursor for Glu, though often MRS studies performed at 3T report Glx, the combination of Glu+Gln signals. N-acetyl aspartyl glutamate (NAAG) functions as a neuromodulator, inhibiting synaptic release of Glu, and dopamine (Harris et al., 2017). Aspartate (Asp) is an excitatory neuromodulator (Menshchikov et al., 2017) and precursor of NAA. Myo-Inositol (mI) acts as an osmolyte, with involvement in maintaining cell volume and fluid balance (Dai et al., 2016) as well as brain cell signaling (Hoyer et al., 2014) and glial cell proliferation (Brand et al., 1993). Scyllo-Inositol (sI) is formed from mI; the functional role of sI in the brain is less clear, though it may decrease accumulation of amyloid-beta protein (McLaurin et al., 2000). The overlapping choline signals (tCho) from free choline, glycerophosphocholine (GPC) and phosphocholine (PCh) are a cell membrane marker which reflects changes in membrane turnover or cell density (Cleeland et al., 2019). Creatine and phosphocreatine (reported in combination as tCr) and lactate (Lac) are all involved in energy metabolism. Creatine is a brain osmolyte and involved in maintenance of brain energy homeostasis (Ross and Sachdev, 2004). Lac is the end product of anaerobic glycolysis, and is found in very low concentrations in the brain under normal physiologic conditions (Harris et al., 2017), but elevated in conditions of altered energy metabolism such as tumor or stroke (Howe et al., 2003; Morana et al., 2015). Glutathione (GSH) is one of the most abundant antioxidant sources in the central nervous system and plays a key role in the maintenance of redox homeostasis (Dwivedi et al., 2020).

A number of cross-sectional studies have characterized the neurometabolic trajectory of aging. Although the results were varied, the most consistent findings demonstrated that NAA and Glu concentration decrease with age, while Cho, Cr and mI concentration increase with age (Cleeland et al., 2019; Haga et al., 2009). Studies using edited MRS methods targeting

specific metabolites have demonstrated an age-related increase in GSH (Hupfeld et al., 2021).

This substantial body of MRS-aging literature has employed diverse methodological approaches, in terms of study design, acquisition, and quantification (Cleeland et al., 2019; Haga et al., 2009). A majority of studies (~65%) has used a dichotomized young-old between-groups design, and of those studies that do consider age as a continuous variable, several have bimodal age distributions. The median total cohort size from previous work is 62 subjects. In terms of acquisition, a majority of studies (~45%) have used PRESS localization for single-voxel acquisitions, whereas some studies (~30%) employed multi-voxel MRSI methods. The quantification approaches range from metabolite ratios (~30%) through water-referenced concentrations with CSF correction (~30%) to full tissue-corrected water referencing (~10%). Given the relatively diverse findings of this literature, which derive in part from limited statistical power, low SNR and methodological diversity, we designed a large structured cross-sectional cohort of male and female subjects throughout adulthood to investigate neurometabolic changes as a function of age, and used data processing, modeling, and quantification practices recommended by recent MRS expert community consensus (Near et al., 2021).

2. Methods

2.1. Participants

One hundred and two healthy volunteers were recruited with local IRB approval (Shandong Provincial Hospital). The cohort was structured to include approximately equal numbers of male and female participants in each decade of age from the 20s, 30s, 40s, 50s, to the 60s. Exclusion criteria included contraindications for MRI and a history of neurological and psychiatric illness. Metabolite-nulled data from the same cohort of subjects was recently published (Hui et al., 2022) to investigate the age trajectory of macromolecular signals in the spectrum. Since this analysis revealed no significant age- or sex-related changes to the macromolecular spectrum, a cohort-mean macromolecule spectrum was incorporated into the modeling (see Analysis).

2.2. MR protocol

Data were acquired on a 3T MRI scanner (Ingenia CX, Philips Healthcare, The Netherlands). Acquisition of MRS data was preceded by a T_1-weighted MPRAGE scan (TR/TE/ 6.9/3.2 ms; FA 8°) with 1 mm^3 isotropic resolution for voxel positioning and tissue segmentation. Metabolite spectra were acquired using PRESS localization (1.3 kHz refocusing bandwidth) with the following parameters: TR/TE: 2000/30 ms; 30 × 26 × 26 mm^3 voxels localized in the CSO (predominantly white matter) and PCC (predominantly gray matter), as shown in Fig. 1; 96 transients sampled at 2 kHz; water suppression was performed using the VAPOR method (Tkác et al., 1999). A slice-selective saturation pulse (20 mm thickness) was applied to suppress subcutaneous lipid adjacent to the voxel in CSO and PCC acquisitions. Water reference spectra were acquired without water suppression or pre-inversion.

2.3. Analysis

T_1-weighted images were segmented using SPM12 (Friston et al., 1994) algorithms called within Osprey (Oeltzschner et al., 2020) after voxel co-registration. Water-suppressed spectra were modeled using the Osprey algorithm, employing a basis set consisting of 18 simulated metabolite basis functions which were generated from a fully localized 2D density-matrix simulation of a 101 × 101 spatial grid (field of view 50% larger than voxel) using real pulse waveforms and sequence timings, as implemented in a MATLAB-based simulation toolbox FID-A (Simpson et al., 2017). Metabolites included in the model are as follows: ascorbate, Asp; creatine, Cr; negative creatine methylene, CrCH2; gamma-aminobutyric acid, GABA; glycerophosphocholine, GPC; glutathione, GSH; glutamine, Gln; glutamate, Glu; myo-inositol, mI; lactate, Lac; N-acetylaspartate, NAA; N-acetylaspartylglutamate, NAAG; phosphocholine, PCh; phosphocreatine, PCr; phosphoethanolamine, PE; scyllo-inositol, sI; and taurine, Tau. GABA was not included in the primary findings, as short-TE PRESS is a controversial approach to measuring GABA levels. Osprey analysis procedures match those previously described in (Zöllner et al., 2021), with the exception that experimentally derived in vivo macromolecular (MM) basis spectra derived from a previous study (Hui et al., 2022) are incorporated into the basis set instead of the eight parameterized Gaussian basis functions. To create the MM basis function, individual-subject ‘clean’ MM spectra (separate for PCC and CSO) were modeled with a flexible spline (0.1 ppm knot spacing) across the full spectral range. The mean of these splines was taken across all subjects (since no significant MM-age relationships were observed before (Hui et al., 2022) to generate the cohort-mean MM basis function. Water reference spectra were modeled with a simulated water basis function in the frequency domain with a 6-parameter model (amplitude, zero- and first-order phase, Gaussian and Lorentzian line-broadening, and frequency shift). Water-referenced metabolite concentrations were calculated according to (Gasparovic et al., 2006), adjusted for tissue-specific water visibility and relaxation times based on literature values (Wansapura et al., 1999) for each segmented tissue fraction of the voxel. Data quality was assessed according to consensus-recommended procedures (Wilson et al., 2019), with a visual inspection of the spectrum, fit, baseline, and residual. Signal-to-noise ratio (SNR) was determined as the ratio of the maximum amplitude of the tNAA signal divided by the standard deviation of the noise, estimated from a de-trended signal-free area of the spectrum. The full-width at half-maximum (FWHM) linewidth of the tNAA signal was also determined.

In order to investigate interactions between changes in linewidth with age, and linear combination modeling, we developed a process to standardize linewidth and SNR across the cohort. First, the 95^{th} percentile values of these metrics were determined for each voxel and set as the target linewidth and SNR. Then, exponential line-broadening was applied to each spectrum to reach the target linewidth. Secondly, the time-modulation of the noise that this introduces was removed by adding back in time-modulated Gaussian noise to return the time-domain noise to its original constant amplitude. Then thirdly, additional time-constant noise was added to reduce the SNR to the target value.

2.4. Statistical Analysis

All statistical analyses were performed using R (Version 4.1.1) in RStudio (Version 1.2.5019, Integrated Development for R. RStudio, PBC, Boston, MA). Data were analyzed for total NAA (tNAA=NAA+NAAG); total choline (tCho=GPC+PCh); total creatine (tCr=Cr+PCr); Glx=Glu+Gln; and individual contributions from Gln, Glu, GSH, mI, Lac, NAA, NAAG, PE, and sI. Concentrations equal to 0 were interpreted as evidence of failure to fit and those datapoints were excluded from further analysis. Normality of metabolite distributions was assessed using the Shapiro-Wilk test. Separate Pearson correlations were run assessing relationship between age and metabolite concentration in each voxel. When the Shapiro-Wilk test indicated that metabolite concentrations were non-normally distributed, Spearman correlations were run to assess the relationship between age and metabolite concentration. Inter-metabolite Spearman correlations were also generated, in order to investigate the degree of positive covariance (potentially driven by biological factors) and negative covariance (driven by modeling 'signal steal'). Paired t-tests were used to investigate regional within-subject concentration differences between the PCC and CSO regions. Robust linear regressions (using Huber M-estimation to downweight influential outliers) were conducted using the MASS package, predicting metabolite concentration from age, sex, and age*sex interaction separately for each voxel. Robust F-tests for multiple coefficients were used to identify impact of each explanatory variable using the sfsmisc package. When significant interactions were found, estimated marginal trends were probed using the emmeans package to assess interaction effects. Finally, to assess the contributions of SNR and FWHM linewidth to metabolite signal, robust linear regressions were conducted with age, SNR, and FWHM linewidth as predictors of metabolite concentration, and robust F-tests were used to identify impact of explanatory variables.

3. Results

Following visual inspection, data were excluded for one subject due to the detection of ethanol signals in the spectra. Data from two further subjects were excluded—one PCC voxel and one CSO voxel—due to the appearance of unacceptably large lipid signals, presumably due to subject motion. The demographic characteristic of final participants are presented in Table 1. The average NAA SNR was 160 in CSO and 150 in PCC, and the average NAA linewidth was 6.8 Hz in CSO and 7.0 Hz in PCC, as shown in Fig. 2, indicating high data quality consistent with the acquisition parameters and the relatively favorable voxel locations. These values fall well within the consensus-recommended limits (Wilson et al., 2019), so no data exclusions were made based on these quality metrics. Across all voxels, amplitude estimates of zero were identified in just three of the considered metabolites—Lac, sI, and PE. Out of 200 total fits, the number of zero-amplitude exclusions for these metabolites was 20, 13, and 1, respectively.

The model results from each region are summarized in Fig. 3 by averaging the individual model results for each decade. Age*metabolite correlation plots for the major metabolites are seen in Fig. 4, and the correlation results are shown in Table 2. Statistically-significant age*metabolite Pearson correlations were observed for tCho ($r(98)=0.33$, $p<0.001$), tCr ($r(98)=0.60$, $p<0.001$), and mI ($r(98)=0.32$, $p=0.001$) in the CSO and for NAAG ($r(98)=0.26$,

p=0.008), tCho(r(98)=0.33, p<0.001), tCr (r(98)=0.39, p<0.001), and Gln (r(98)=0.21, p=0.034) in the PCC. The Shapiro-Wilk test revealed non-normal distribution of NAA (W=0.97, p=0.015), sI (W=0.94, p<0.001) and Lac (W=0.84, p<0.001) in the CSO and sI (W=0.95, p=0.0015), Lac (W=0.91, p<0.001), and Asp (W=0.96, p=0.005) in the PCC. Therefore, the relationship between these metabolites and age was assessed instead using Spearman correlations. sI was significantly correlated with age in the CSO (r(86)=0.26, p=0.013), but not the PCC. No significant correlations were seen between tNAA, NAA, Glx, Glu, GSH, PE, Lac, or Asp and age in either region (all p>0.20). Age correlations and inter-metabolite correlations are illustrated in Fig. 5.

Paired t-test results indicated levels of NAA (t(98)=−7.65, p<0.001), tCr (t(98)=−44.49, p<0.001), mI (t(98)=−38.09, p<0.001), Glx (t(98)=−29.90, p<0.001), Glu (t(98)=−30.91, p<0.001), Gln (t(98)=−24.51, p<0.001), GSH (t(98)=−16.25, p<0.001), sI (t(85)=−13.80, p<0.001), Lac (t(79)=−3.81, p<0.001), and Asp (t(97)=−18.41, p<0.001) were significantly higher in the PCC compared with the CSO. tNAA (t(98)=6.40, p<0.001), NAAG (t(98)=24.56, p<0.001), and tCho (t(98)=26.57, p<0.001), were significantly higher in the CSO compared with the PCC. No difference in PE concentration between voxels was observed (p>0.05).

Initial robust linear regressions assessed the independent contributions of age and sex to metabolite concentrations in individual voxels (Table 3). When controlling for sex, age remained significantly associated with CSO concentrations of tCho (F(1,97)=14.24, p<0.001), tCr (F(1,97)=60.42, p<0.001), mI (F(1,97)=13.40, p<0.001), and sI (F(1,85)=8.90, p=0.004). In the PCC, when controlling for sex, age was significantly associated with NAAG (F(1,97)=9.10, p=0.003), tCho (F(1,97)=12.21, p=0.001), and tCr (F(1,97)=20.77, p<0.001). A significant main effect of sex was observed in the CSO for NAAG (F(1,97)=6.63, p=0.012) and Asp (F(1,96)=4.54, p =0.036). Post hoc pairwise comparisons of estimated marginal means revealed that both NAAG (p=0.010) and Asp (p=0.033) concentrations were higher in women compared with men. In the PCC, a significant main effect of sex was observed for tNAA (F(1,97)=5.60, p=0.020), Gln (F(1,97)=5.21, p=0.025), sI (F(1,96)=17.40, p<0.001), and Lac (F(1,79)=5.19, p=0.025). Post hoc pairwise comparisons of estimated marginal means revealed that concentrations of tNAA (p=0.018), sI (p<0.001), and Lac (p=0.023) were all higher in women compared with men, and that Gln Gln (p=0.023) was higher in men compared with women.

In follow-up robust linear regressions, we also added an age*sex interaction term to probe the effect of age, sex, and age*sex interaction on metabolite concentrations in individual voxels. Full results from this model are reported in Table 4. Significant age*sex interaction effects were observed for tCho (F(1,96)=11.53, p=0.001) and GSH (F(1,96)=7.15, p=0.009) in the CSO. Post-hoc examination of estimated marginal trends revealed that tCho and GSH increased with age in women, but not men. In the PCC, significant age*sex interaction effects were observed for tCho (F(1,96)=9.17, p=0.003), tCr(F(1,96)=9.59, p=0.003), mI (F(1,96)=6.48, p=0.012), and Lac (F(1,78)=6.04, p=0.016). Examination of estimated marginal trends indicated that tCho, tCr, mI, and Lac increased with age in women, but not in men.

There was a significant positive correlation between linewidth and age, as seen in Fig. 2, with older subjects tending to have broader signals. This was also reflected in SNR (peak height being inversely related to linewidth for a given area), as expected. After the data were manipulated to standardize linewidth and SNR to the 95th percentile values, these strong correlations are no longer seen. Correlations between metabolite measures before and after linewidth/SNR adjustment procedure were as shown in supplemental Fig. S1. Metabolite measures plotted against age before linewidth/SNR adjustment and after were indicated in supplemental Fig. S2. In these manipulated data, robust linear regressions (Table 5) indicated that age was significantly associated with tCho ($F(1,96)=15.14$, $p<0.001$), tCr($F(1,96)=37.52$, $p<0.001$), and mI ($F(1,96)=7.12$, $p=0.009$) in the CSO and tCho ($F(1,96)=8.01$, $p=0.006$), tCr ($F(1,96)=27.96$, $p<0.001$), mI ($F(1,96)=5.80$, $p=0.018$), and sI ($F(1,95)=5.18$, $p=0.025$) in the PCC. SNR was associated with tNAA ($F(1,96)=29.32$, $p<0.001$), NAA ($F(1,96)=13.96$), $p<0.001$), NAAG ($F(1,96)=18.84$, $p<0.001$), tCho ($F(1,96)=14.68$, $p<0.001$), mI ($F(1,96)=4.75$, $p=0.032$), PE ($F(1,96)=4.44$, $p=0.038$), and Asp ($F(1,95)=9.49$, $p=0.003$) in the CSO. No associations between SNR and metabolite levels in the PCC reached statistical significance ($p > 0.05$). FWHM was significantly associated with tCho ($F(1,96)=5.68$, $p=0.019$) and PE ($F(1,96)=8.75$, $p=0.004$) in the CSO and with NAAG ($F(1,96)=4.99$, $p=0.028$), tCr ($F(1,96)=7.76$, $p=0.006$), mI ($F(1,96)=4.08$, $p=0.046$), and PE ($F(1,95)=12.39$, $p=0.001$) in the PCC. The correlations between tissue fraction of the two selected voxels and age was reported in (Hui et al., 2022) with reference to MM spectra acquired in the same cohort.

4. Discussion

In this study, MRS data from a large structured cross-sectional cohort of male and female subjects throughout adulthood were investigated for neurometabolic changes as a function of age, using MRS consensus-recommended quantification methods (Near et al., 2021; Wilson et al., 2019). Positive age correlations in tCho and tCr were observed for CSO and PCC, while mI and sI levels increased with aging only in CSO, and NAAG and Gln levels were increased with aging only in PCC. No age correlations were found for tNAA, NAA, Glx, Glu, GSH, PE, Lac, or Asp in either region. Together, our results provide a normative assessment of the trajectories of MRS-measured metabolite levels in CSO and PCC across the healthy adult lifespan.

This study indicated that tCho and tCr increased with age in both CSO and PCC, in line with most previous MRS studies (Cleeland et al., 2019), perhaps driven by glial proliferation, as higher Cho and Cr levels are found in glial cells (Brand et al., 1993). The glial metabolite mI demonstrated a positive correlation with age in CSO, while no mI correlations with age were found in PCC. The metabolically linked sI showed an increase in CSO and no effect in PCC, in line with prior work (Kaiser et al., 2005). sI was also significantly higher in the PCC in female subjects, suggesting sex should be considered when investigating sI alterations.

The relatively strong positive correlations between tCr levels and age suggest that more age-related declines in metabolite levels would be reported if Cr-referenced metabolite ratios were used for quantification. While the quantification approach used here (relaxation and tissue correction based on literature reference values) complies with community consensus

(Near et al., 2021; Wilson et al., 2019), it is still not free from potential confounds. There is strong literature evidence of age-related changes in the relaxation rates of water signals (Knight et al., 2016; Söderberg et al., 1990) and metabolite signals (Deelchand et al., 2020; Kirov et al., 2008; McIntyre et al., 2007; Schenker et al., 1993), that are not considered by the quantification approach used here. There is a strong need in the community for age-normed reference values to address this deficiency.

It is notable that age correlations were not observed for NAA, tNAA, Glu and Glx in either region, in spite of the fact that this is one of the commonest findings in the literature (Cleeland et al., 2019). In addition, no age-related changes in GSH were observed, in contrast to the edited MRS literature (Hupfeld et al., 2021). One potential explanation for the lack of age effects for these metabolites is the age-range of our cohort (20-69 years), which would not be sensitive to changes later in life, such as those reported in previous cohorts (60-85 years) (Suri et al., 2017) and (60-90 years) (Sijens et al., 2003) . NAA and Glu declines often seen in metabolite ratios – most often ratios to Cr – and so might be driven by the reference denominator as much as changes in the numerator. It may also be the case that non-linear metabolite by age relationships will be revealed in studies of wider age ranges, as we recently reported in a meta-analysis of edited GABA MRS across the lifespan (Porges et al., 2021). The majority of studies applying relaxation and tissue correction do not show age-related NAA changes (Wu et al., 2012). However, a recent study applying absolute quantification by phantom (Kirov et al., 2021) did report decreases in whole-brain NAA concentration with age. This cohort included a large number of subjects above the age range of our cohort, so the difference in findings could be driven by either cohort, regional variation or methodology.

In addition, main effects of sex were observed in initial robust linear models, such that in the CSO NAAG and Asp were higher for females and in the PCC tNAA, sI, and Lac were higher for females, while Gln was higher for males. Probing age*sex interaction with follow-up models indicated that in females only, tCho and GSH increased with age in the CSO and tCho, tCr, mI, and Lac increased with age in the PCC. Many previous reports on MRS-measured metabolite changes with aging include approximately equal numbers of males and females, but either find no sex effects (Ding et al., 2016; Marjańska et al., 2017) or do not report on sex differences (Hupfeld et al., 2021; Suri et al., 2017)—making comparisons with the present work challenging. One prior study of 30 adults ages 22-82 similarly found higher PCC tCr in females compared with males, but no other sex effects (Chiu et al., 2014). However, work in 118 individuals ages 20-56 years found higher tCho and tCr for males in the anterior cingulate cortex but lower tCr for males in the hippocampus (Hädel et al., 2013), suggesting that sex effects on these metabolite levels may differ by brain region. Another prior study of 117 middle- to older-age adults (43-89 years) found conflicting results of lower parietal tCho and mi for women compared with men (Williamson et al., 2021). Taken together, sex contributions to changes in metabolite levels with aging remain unclear and require replication in future large samples.

The manipulation of data to remove age-related changes in linewidth and SNR is an experimental approach that demands further investigation before widespread adoption. Given this status, we consider the results from unmanipulated data as the primary results

in this manuscript. Standardization of linewidth and SNR does not greatly change the age relationships seen among the metabolites, but it does result in some cases in significant changes (both positive and negative) to measured metabolite levels and the correlations between metabolite levels before and after manipulation are ~0.7 (higher for more prominent signals, and lower for more coupled signals), as shown in supplemental Fig.s.

The inter-metabolite correlations reveal some interesting relationships. Overall, there are more positive than negative correlations. While there is a concern that common variance in the reference signal drive such correlations, they do not appear to be more prevalent within-region (common reference) compared to between region (independent reference). We therefore interpret this as reflecting genuine biological co-variance. Several metabolites showed substantial positive correlations between PCC and CSO - tCho, tCr, mI, and sI. Negative correlations between metabolites with overlapping basis spectra are potential evidence of the limitation of linear-combination modeling at 3T. These is seen between GSH and PE, exclusively within-region.

We used the publicly available Osprey algorithm for perform linear-combination modeling of our data. While similar in concept, implementation and performance to the de-facto gold standard LCModel and other widely used methods like Tarquin (Wilson et al., 2011), we have recently demonstrated that results obtained with different modeling algorithms might differ in systematic fashion (Zöllner et al., 2021), a phenomenon commonly encountered in many neuroimaging disciplines. One key algorithmic difference is that the Osprey algorithm does not apply soft constraints to regularize the contributions from typically low-concentration metabolites like GSH, as is done by the LCModel, which may decrease systematic biases.

There are some limitations in this study, first, even though an ade-quate sample size was achieved, the age span was relatively narrow. In particular, we did not enroll participants above 70 years of age, i.e. when effects of aging drastically accelerate. Future MRS-aging studies should increase the age range to establish normative age trajectories during this important late-life stage. Second, only two selected ROIs (PCC and CSO) were analyzed in this study, one is gray-matter predominant region, another white-matter predominant. Neurochemical changes during aging are highly region-dependent (Eylers et al., 2016), and data from more regions or even whole brain data will be needed to improve our understanding of age-related changes.

5. Conclusion

The results indicated positive age correlations for tCho, tCr, sI, and mI in the CSO and for NAAG, tCho, tCr and Gln in the PCC, but no age correlations for for tNAA, NAA, Glx, Glu, GSH, PE, Lac, or Asp in either region. Our results provide further evidence of neurometabolic time course of healthy aging, suggesting that age matching is essential for comparative studies of neurodegenerative disease using MRS.

Supplementary Material

Refer to Web version on PubMed Central for supplementary material.

Acknowledgements

This work was supported by Natural Science Foundation of Shandong (grant number: ZR2020QH267); China Postdoctoral Science Foundation (grant number: 2022M711987); Major Research Project of Shandong Province (grant number: 2016ZDJS07A16); Academic promotion program of Shandong First Medical University (grant number: 2019QL023); and National Institutes of Health (grant number: R01 EB016089; R21 AG060245; P41 EB031771; R00 AG062230; K00 AG068440).

Data availability

Data will be made available on request.

References

Brand A, Richter-Landsberg C, Leibfritz D, 1993. Multinuclear NMR studies on the energy metabolism of glial and neuronal cells. DNE 15, 289–298. doi:10.1159/000111347.

Cheng H, Wang A, Newman S, Dydak U, 2021. An investigation of glutamate quantification with PRESS and MEGA-PRESS. NMR Biomed. 34, e4453. doi:10.1002/nbm.4453. [PubMed: 33617070]

Chiu P-W, Mak HK-F, Yau KK-W, Chan Q, Chang RC-C, Chu L-W, 2014. Metabolic changes in the anterior and posterior cingulate cortices of the normal aging brain: proton magnetic resonance spectroscopy study at 3 T. AGE 36, 251–264. doi:10.1007/s11357-013-9545-8. [PubMed: 23709317]

Cleeland C, Pipingas A, Scholey A, White D, 2019. Neurochemical changes in the aging brain: a systematic review. Neurosci. Biobehav. Rev 98, 306–319. doi:10.1016/j.neubiorev.2019.01.003. [PubMed: 30625337]

Dai G, Yu H, Kruse M, Traynor-Kaplan A, Hille B, 2016. Osmoregulatory inositol transporter SMIT1 modulates electrical activity by adjusting PI(4,5)P2 levels. Proc. Natl. Acad. Sci. USA 113, E3290–E3299. doi:10.1073/pnas.1606348113. [PubMed: 27217553]

Deelchand DK, McCarten JR, Hemmy LS, Auerbach EJ, Eberly LE, Marjańska M, 2020. Changes in the intracellular microenvironment in the aging human brain. Neurobiol. Aging 95, 168–175. doi:10.1016/j.neurobiolaging.2020.07.017. [PubMed: 32814258]

Ding X-Q, Maudsley AA, Sabati M, Sheriff S, Schmitz B, Schütze M, Bronzlik P, Kahl KG, Lanfermann H, 2016. Physiological neuronal decline in healthy aging human brain — an in vivo study with MRI and short echo-time whole-brain 1H MR spectroscopic imaging. Neuroimage 137, 45–51. doi:10.1016/j.neuroimage.2016.05.014. [PubMed: 27164326]

Dwivedi D, Megha K, Mishra R, Mandal PK, 2020. Glutathione in brain: overview of its conformations, functions, biochemical characteristics, quantitation and potential therapeutic role in brain disorders. Neurochem. Res 45, 1461–1480. doi:10.1007/s11064-020-03030-1. [PubMed: 32297027]

Eylers VV, Maudsley AA, Bronzlik P, Dellani PR, Lanfermann H, Ding X-Q, 2016. Detection of normal aging effects on human brain metabolite concentrations and microstructure with whole-brain MR spectroscopic imaging and quantitative MR imaging. Am. J. Neuroradiol 37, 447–454. doi:10.3174/ajnr.A4557. [PubMed: 26564440]

Friston KJ, Holmes AP, Worsley KJ, Poline J-P, Frith CD, Frackowiak RSJ, 1994. Statistical parametric maps in functional imaging: a general linear approach. Hum. Brain Mapp 2, 189–210. doi:10.1002/hbm.460020402.

Gasparovic C, Song T, Devier D, Bockholt HJ, Caprihan A, Mullins PG, Posse S, Jung RE, Morrison LA, 2006. Use of tissue water as a concentration reference for proton spectroscopic imaging. Magn. Reson. Med 55, 1219–1226. doi:10.1002/mrm.20901. [PubMed: 16688703]

Hädel S, Wirth C, Rapp M, Gallinat J, Schubert F, 2013. Effects of age and sex on the concentrations of glutamate and glutamine in the human brain: brain glutamate and glutamine with age and sex. J. Magn. Reson. Imaging 38, 1480–1487. doi:10.1002/jmri.24123. [PubMed: 23564615]

Haga KK, Khor YP, Farrall A, Wardlaw JM, 2009. A systematic review of brain metabolite changes, measured with 1H magnetic resonance spectroscopy, in healthy aging. Neurobiol. Aging 30, 353–363. doi:10.1016/j.neurobiolaging.2007.07.005. [PubMed: 17719145]

Harris AD, Saleh MG, Edden RAE, 2017. Edited 1H magnetic resonance spectroscopy in vivo: methods and metabolites. Magn. Reson. Med 77, 1377–1389. doi:10.1002/mrm.26619. [PubMed: 28150876]

Howe FA, Barton SJ, Cudlip SA, Stubbs M, Saunders DE, Murphy M, Wilkins P, Opstad KS, Doyle VL, McLean MA, Bell BA, Griffiths JR, 2003. Metabolic profiles of human brain tumors using quantitative in vivo1H magnetic resonance spectroscopy. Magn. Reson. Med 49, 223–232. doi:10.1002/mrm.10367. [PubMed: 12541241]

Hoyer C, Gass N, Weber-Fahr W, Sartorius A, 2014. Advantages and challenges of small animal magnetic resonance imaging as a translational tool. NPS 69, 187–201. doi:10.1159/000360859.

Hui SCN, Gong T, Zöllner HJ, Song Y, Murali-Manohar S, Oeltzschner G, Mikkelsen M, Tapper S, Chen Y, Saleh MG, Porges EC, Chen W, Wang G, Edden RAE, 2022. The macromolecular MR spectrum does not change with healthy aging. Magn. Reson. Med 87, 1711–1719. doi:10.1002/mrm.29093. [PubMed: 34841564]

Hupfeld KE, Hyatt HW, Alvarez Jerez P, Mikkelsen M, Hass CJ, Edden RAE, Seidler RD, Porges EC, 2021. In vivo brain glutathione is higher in older age and correlates with mobility. Cereb. Cortex 31, 4576–4594. doi:10.1093/cercor/bhab107. [PubMed: 33959751]

Kaiser LG, Schuff N, Cashdollar N, Weiner MW, 2005. Scyllo-inositol in normal aging human brain: 1H magnetic resonance spectroscopy study at 4 Tesla. NMR Biomed. 18, 51–55. doi:10.1002/nbm.927. [PubMed: 15468140]

Kirov II, Fleysher L, Fleysher R, Patil V, Liu S, Gonen O, 2008. The age dependence of regional proton metabolites T2 relaxation times in the human brain at 3 Tesla. Magn. Reson. Med 60, 790–795. doi:10.1002/mrm.21715. [PubMed: 18816831]

Kirov II, Sollberger M, Davitz MS, Glodzik L, Soher BJ, Babb JS, Monsch AU, Gass A, Gonen O, 2021. Global brain volume and N-acetyl-aspartate decline over seven decades of normal aging. Neurobiol. Aging 98, 42–51. doi:10.1016/j.neurobiolaging.2020.10.024. [PubMed: 33232854]

Knight MJ, McCann B, Tsivos D, Couthard E, Kauppinen RA, 2016. Quantitative T1 and T2 MRI signal characteristics in the human brain: different patterns of MR contrasts in normal ageing. MAGMA 29, 833–842. doi:10.1007/s10334-016-0573-0. [PubMed: 27333937]

Landim RCG, Edden RAE, Foerster B, Li LM, Covolan RJM, Castellano G, 2016. Investigation of NAA and NAAG dynamics underlying visual stimulation using MEGA-PRESS in a functional MRS experiment. Magn. Reson. Imaging 34, 239–245. doi:10.1016/j.mri.2015.10.038. [PubMed: 26656908]

Langa KM, Larson EB, Wallace RB, Fendrick AM, Foster NL, Kabeto MU, Weir DR, Willis RJ, Herzog AR, 2004. Out-of-pocket health care expenditures among older Americans with dementia. Alzheimer Dis. Assoc. Disord 18, 90–98. doi:10.1097/01.wad.0000126620.73791.3e. [PubMed: 15249853]

Marjańska M, McCarten JR, Hodges J, Hemmy LS, Grant A, Deelchand DK, Terpstra M, 2017. Region-specific aging of the human brain as evidenced by neurochemical profiles measured noninvasively in the posterior cingulate cortex and the occipital lobe using 1 H magnetic resonance spectroscopy at 7 T. Neuroscience 354, 168–177. doi:10.1016/j.neuroscience.2017.04.035. [PubMed: 28476320]

McIntyre DJO, Charlton RA, Markus HS, Howe FA, 2007. Long and short echo time proton magnetic resonance spectroscopic imaging of the healthy aging brain. J. Magn. Reson. Imaging 26, 1596–1606. doi:10.1002/jmri.21198. [PubMed: 17968966]

McLaurin J, Golomb R, Jurewicz A, Antel JP, Fraser PE, 2000. Inositol stereoisomers stabilize an oligomeric aggregate of alzheimer amyloid β peptide and inhibit Aβ-induced toxicity *. J. Biol. Chem 275, 18495–18502. doi:10.1074/jbc.M906994199. [PubMed: 10764800]

Menshchikov PE, Akhadov TA, Semenova NA, 2017. Quantification of cerebral aspartate concentration in vivo using proton magnetic resonance spectroscopy. Bull. Lebedev Phys. Inst 44, 56–60. doi:10.3103/S1068335617030022.

Morana G, Piccardo A, Puntoni M, Nozza P, Cama A, Raso A, Mascelli S, Massollo M, Milanaccio C, Garrè ML, Rossi A, 2015. Diagnostic and prognostic value of 18F-DOPA PET and 1H-MR spectroscopy in pediatric supratentorial infiltrative gliomas: a comparative study. Neuro-oncol. 17, 1637–1647. doi:10.1093/neuonc/nov099. [PubMed: 26405202]

Near J, Harris AD, Juchem C, Kreis R, Marjańska M, Öz G, Slotboom J, Wilson M, Gasparovic C, 2021. Preprocessing, analysis and quantification in single-voxel magnetic resonance spectroscopy: experts' consensus recommendations. NMR Biomed. 34, e4257. doi:10.1002/nbm.4257. [PubMed: 32084297]

Oeltzschner G, Zöllner HJ, Hui SCN, Mikkelsen M, Saleh MG, Tapper S, Edden RAE, 2020. Osprey: open-source processing, reconstruction & estimation of magnetic resonance spectroscopy data. J. Neurosci. Methods 343, 108827. doi:10.1016/j.jneumeth.2020.108827. [PubMed: 32603810]

Porges EC, Jensen G, Foster B, Edden RA, Puts NA, 2021. The trajectory of cortical GABA across the lifespan, an individual participant data meta-analysis of edited MRS studies. eLife 10, e62575. doi:10.7554/eLife.62575. [PubMed: 34061022]

Ross AJ, Sachdev PS, 2004. Magnetic resonance spectroscopy in cognitive research. Brain Res. Rev 44, 83–102. doi:10.1016/j.brainresrev.2003.11.001. [PubMed: 15003387]

Schenker C, Meier D, Wichmann W, Boesiger P, Valavanis A, 1993. Age distribution and iron dependency of the T2 relaxation time in the globus pallidus and putamen. Neuroradiology 35, 119–124. doi:10.1007/BF00593967. [PubMed: 8433786]

Sijens PE, Heijer T.den, Origgi D, Vermeer SE, Breteler MMB, Hofman A, Oudkerk M, 2003. Brain changes with aging: MR spectroscopy at supraventricular plane shows differences between women and men. Radiology 226, 889–896. doi:10.1148/radiol.2263011937. [PubMed: 12601215]

Simpson R, Devenyi GA, Jezzard P, Hennessy TJ, Near J, 2017. Advanced processing and simulation of MRS data using the FID appliance (FID-A)-An open source, MATLAB-based toolkit. Magn. Reson. Med 77, 23–33. doi:10.1002/mrm.26091. [PubMed: 26715192]

Söderberg M, Edlund C, Kristensson K, Dallner G, 1990. Lipid compositions of different regions of the human brain during aging. J. Neurochem 54, 415–423. doi:10.1111/j.1471-4159.1990.tb01889.x. [PubMed: 2299344]

Suri S, Emir U, Stagg CJ, Near J, Mekle R, Schubert F, Zsoldos E, Mahmood A, Singh-Manoux A, Kivimäki M, Ebmeier KP, Mackay CE, Filippini N, 2017. Effect of age and the APOE gene on metabolite concentrations in the posterior cingulate cortex. Neuroimage 152, 509–516. doi:10.1016/j.neuroimage.2017.03.031. [PubMed: 28323160]

Tkác I, Starcuk Z, Choi IY, Gruetter R, 1999. In vivo 1H NMR spectroscopy of rat brain at 1 ms echo time. Magn. Reson. Med 41, 649–656. doi:10.1002/(sici)1522-2594(199904)41:4<649::aid-mrm2>3.0.co;2-g. [PubMed: 10332839]

Wansapura JP, Holland SK, Dunn RS, Ball WS Jr., 1999. NMR relaxation times in the human brain at 3.0 tesla. J. Magn. Reson. Imaging 9, 531–538. doi:10.1002/(SICI)1522-2586(199904)9:4<531::AID-JMRI4>3.0.CO;2-L. [PubMed: 10232510]

Williamson JB, Lamb DG, Porges EC, Bottari S, Woods AJ, Datta S, Langer K, Cohen RA, 2021. Cerebral metabolite concentrations are associated with cortical and subcortical volumes and cognition in older adults. Front. Aging Neurosci 12, 587104. doi:10.3389/fnagi.2020.587104. [PubMed: 33613261]

Wilson M, Andronesi O, Barker PB, Bartha R, Bizzi A, Bolan PJ, Brindle KM, Choi I-Y, Cudalbu C, Dydak U, Emir UE, Gonzalez RG, Gruber S, Gruetter R, Gupta RK, Heerschap A, Henning A, Hetherington HP, Huppi PS, Hurd RE, Kantarci K, Kauppinen RA, Klomp DWJ, Kreis R, Kruiskamp MJ, Leach MO, Lin AP, Luijten PR, Marjańska M, Maudsley AA, Meyerhoff DJ, Mountford CE, Mullins PG, Murdoch JB, Nelson SJ, Noeske R, Öz G, Pan JW, Peet AC, Poptani H, Posse S, Ratai E-M, Salibi N, Scheenen TWJ, Smith ICP, Soher BJ, Tkáč I, Vigneron DB, Howe FA, 2019. Methodological consensus on clinical proton MRS of the brain: review and recommendations. Magn. Reson. Med 82, 527–550. doi:10.1002/mrm.27742. [PubMed: 30919510]

Wilson M, Reynolds G, Kauppinen RA, Arvanitis TN, Peet AC, 2011. A constrained least-squares approach to the automated quantitation of in vivo ^{1}H magnetic resonance spectroscopy data. Magn. Reson. Med 65, 1–12. doi:10.1002/mrm.22579. [PubMed: 20878762]

Wu WE, Gass A, Glodzik L, Babb JS, Hirsch J, Sollberger M, Achtnichts L, Amann M, Monsch AU, Gonen O, 2012. Whole brain N-acetylaspartate concentration is conserved throughout normal aging. Neurobiol. Aging 33, 2440–2447. doi:10.1016/j.neurobiolaging.2011.12.008. [PubMed: 22245316]

Zöllner HJ, Považan M, Hui SCN, Tapper S, Edden RAE, Oeltzschner G, 2021. Comparison of different linear-combination modeling algorithms for short-TE proton spectra. NMR Biomed. 34, e4482. doi:10.1002/nbm.4482. [PubMed: 33530131]

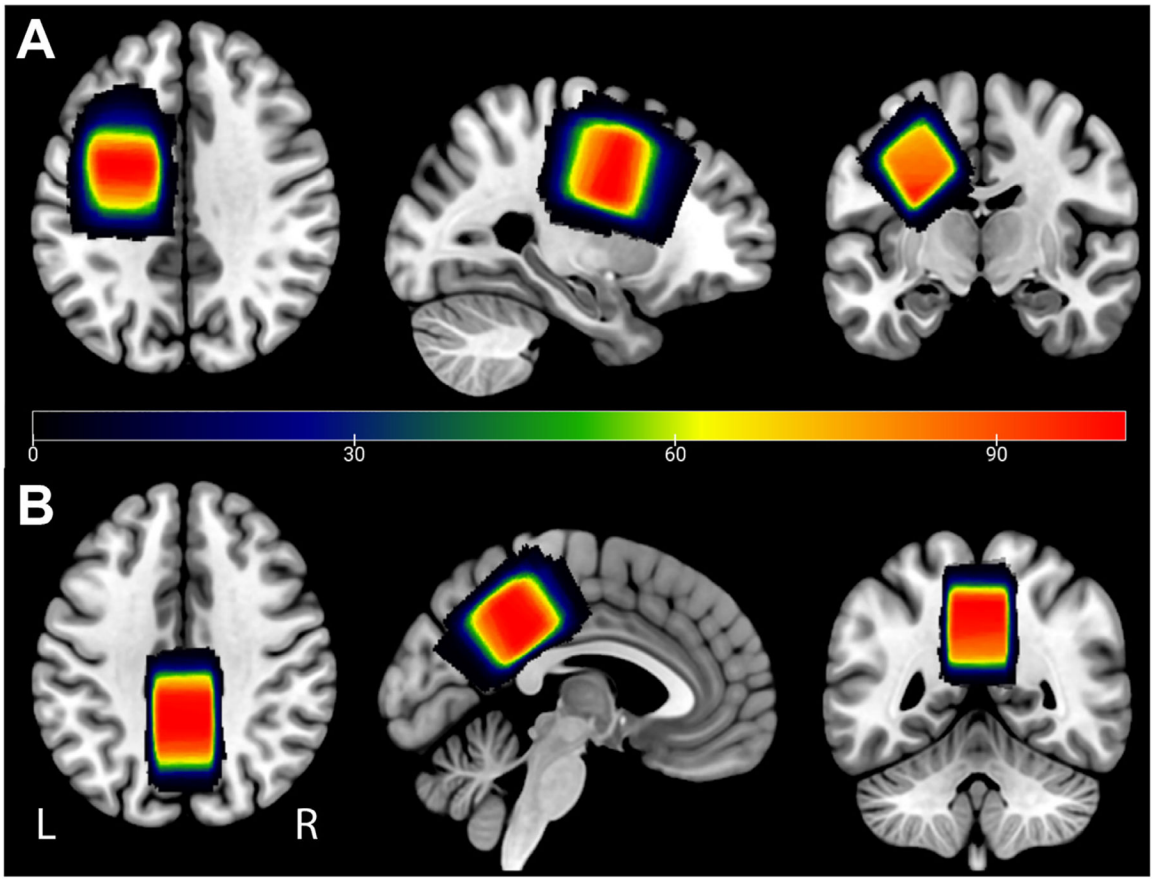

Fig. 1.

Voxels of interest a) left CSO and b) midline PCC in which spectral data were acquired. Acquisition parameters: 96 transients; TR=2s; TE=30 ms; 20 cm^3 voxels. Here we depict each participan's native space binary voxel mask normalized to MNI space and overlaid onto the spm152 template. Warmer colors indicate areas of greater overlap across participants.

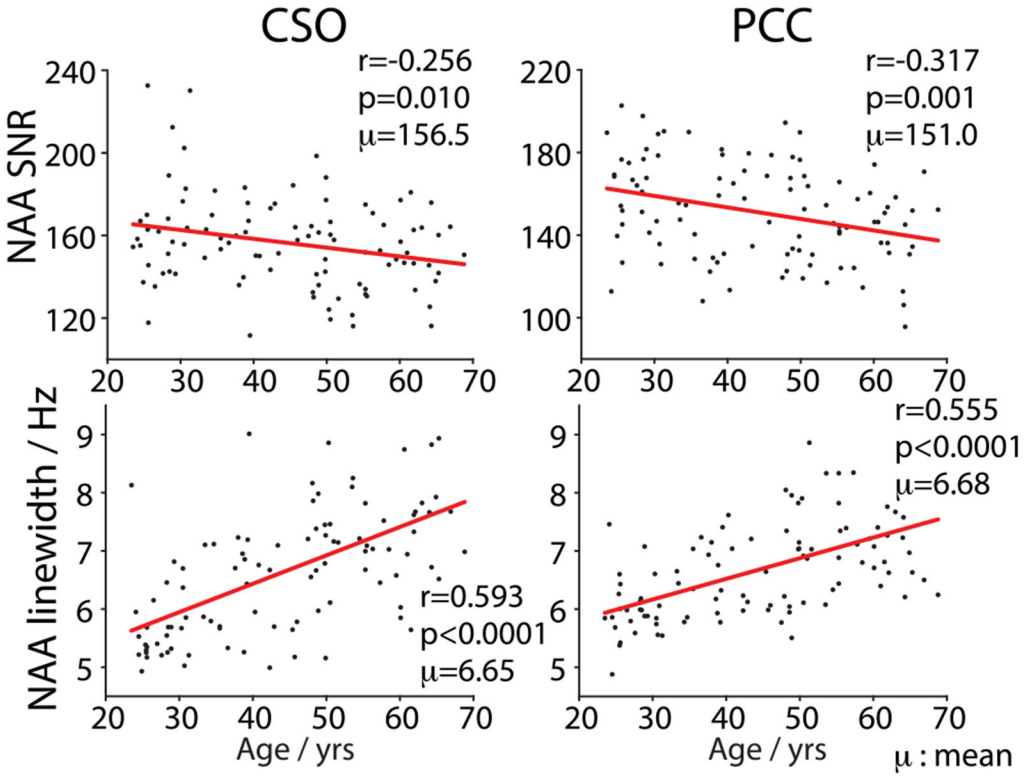

Fig. 2.
Correlations of age with the SNR and linewidth metrics of NAA. μ=mean.

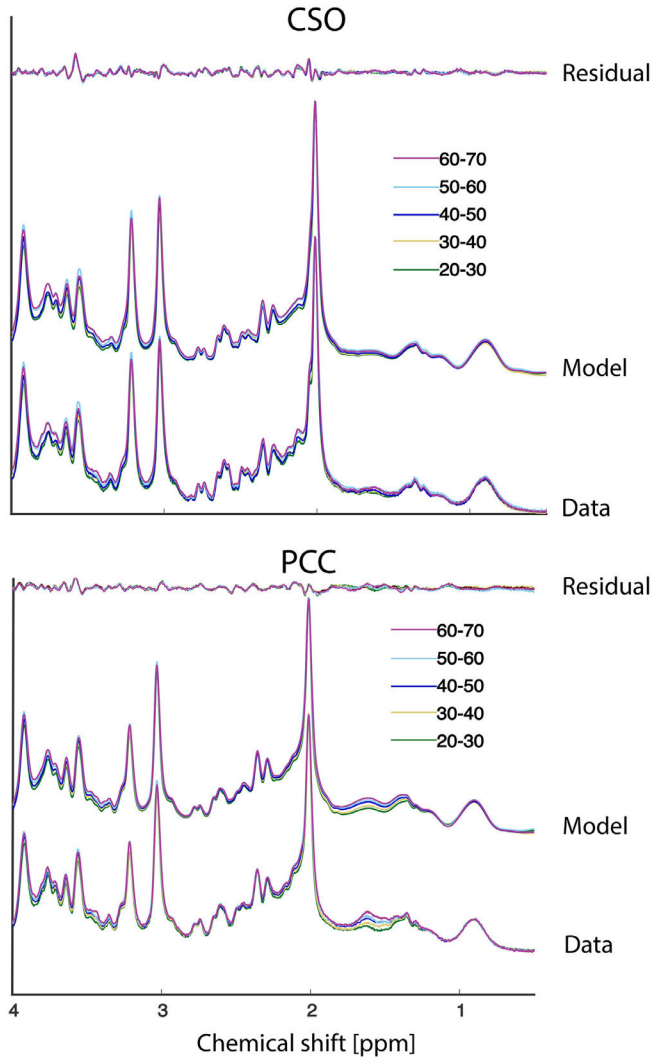

Fig. 3.

Average model results (averaged across model results of each subject) per decade from CSO (upper panel) and PCC (lower panel). The residual is defined as the difference between the data and the model.

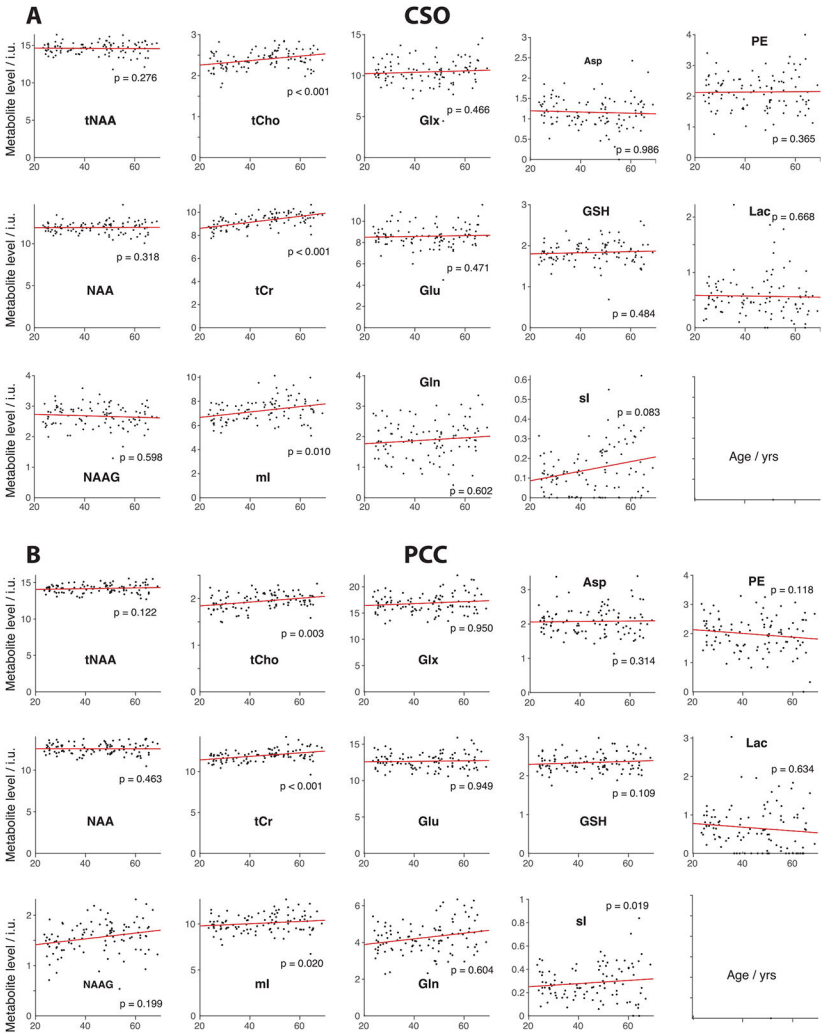

Fig. 4.

Metabolite-age correlation plots from (a) CSO and (b) PCC.

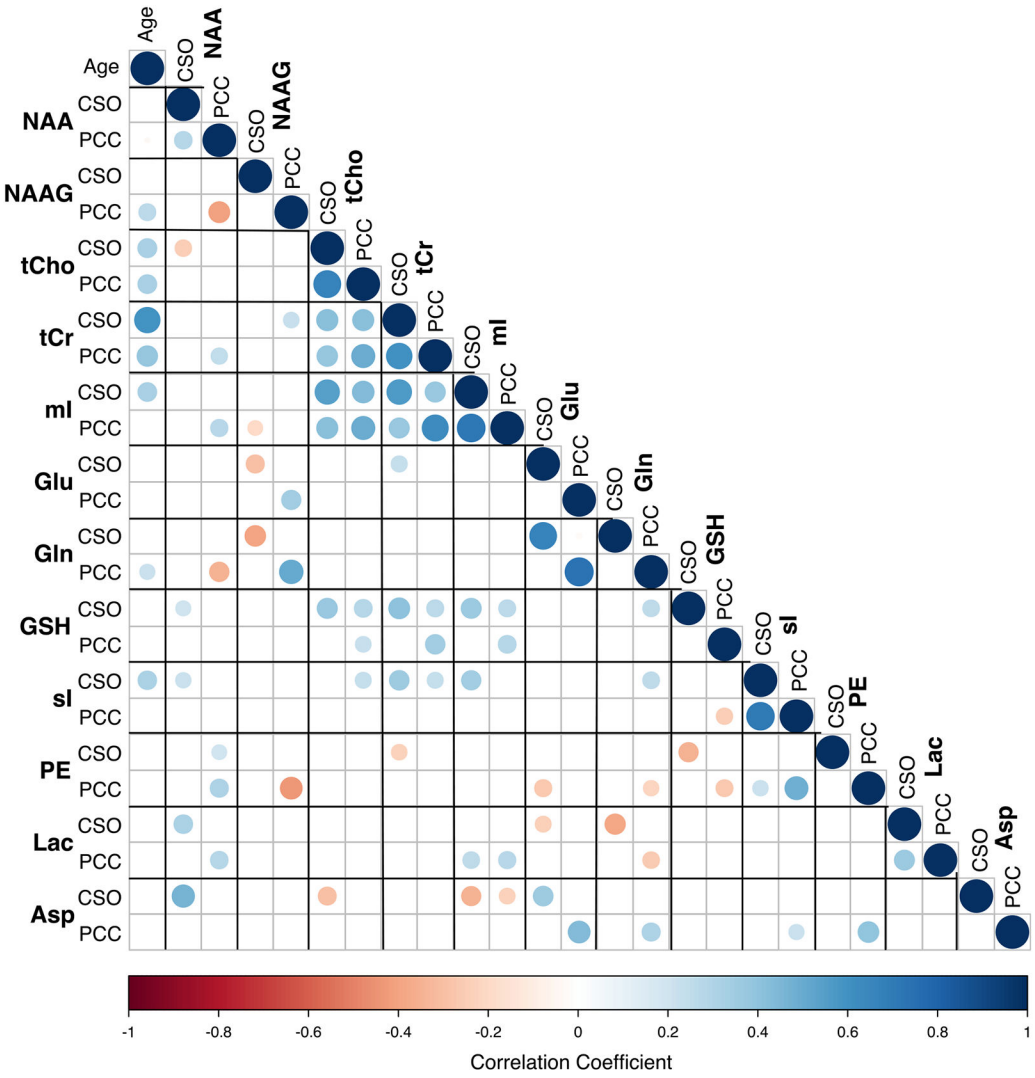

Fig. 5.

Age correlations and inter-metabolite correlations. Dot radius and color indicate correlation strength (according to the color bar), while color indicates correlation directionality.

Table 1

Demographic characteristics of all participants

	20s (*n*=21)	30s (*n*=21)	40s (*n*=20)	50s (*n*=20)	60s (*n*=20)	Total (*n*=102)
Age (years)						
Mean	26.0	34.6	45.7	53.9	63.6	44.5
Sex, *n*						
Male	10	10	10	10	9	49
Female	11	11	10	10	11	53

Table 2

Mean metabolite levels in institutional units and correlations between age and metabolite concentrations by voxel.

	CSO				PCC			
Metabolite	***n***	**Mean (SD)**	**r**	**p**	***n***	**Mean (SD)**	**r**	**p**
tNAA	100	14.67 (0.72)	0.041	0.68	100	14.17 (0.60)	0.093	0.36
NAA*	100	11.96 (0.64)	0.098	0.33	100	12.56 (0.65)	−0.027	0.79
NAAG	100	2.70 (0.33)	−0.047	0.64	100	1.56 (0.32)	0.26	**0.008**
tCho	100	2.39 (0.22)	0.33	**<0.001**	100	1.94 (0.17)	0.33	**<0.001**
tCr	100	9.27 (0.61)	0.60	**<0.001**	100	11.94 (0.71)	0.39	**<0.001**
mI	100	7.23 (0.97)	0.32	**0.001**	100	10.08 (0.99)	0.17	0.087
Glx	100	10.52 (1.39)	0.11	0.28	100	16.81 (1.73)	0.10	0.31
Glu	100	8.64 (0.93)	0.08	0.42	100	12.62 (1.04)	0.002	0.98
Gln	100	1.91 (0.60)	0.13	0.20	100	4.23 (0.82)	0.21	**0.034**
GSH	100	1.85 (0.24)	0.13	0.21	100	2.34 (0.23)	0.13	0.20
sI*	88	0.16 (0.11)	0.26	**0.013**	99	0.29 (0.14)	0.18	0.076
PE	100	2.13 (0.54)	−0.028	0.78	99	2.00 (0.58)	−0.11	0.27
Lac*	98	0.58 (0.36)	−0.032	0.76	82	0.81 (0.50)	0.042	0.70
Asp*	99	1.18 (0.35)	−0.083	0.41	100	2.08 (0.40)	0.022	0.83

Note: Metabolite concentrations were normally distributed and Pearson correlations reported in all cases except those indicated by *; in these cases, metabolite concentrations were not normally distributed and Spearman correlations were used.

Table 3

Robust linear regressions and robust F-tests assessing separate contributions of sex and age (without the age*sex interaction term) to metabolite concentrations within each voxel. Coefficients represent robust regressions; F- and p-values are derived from robust F-tests. CSO results are presented first, followed by PCC results.

CSO						
	Age			**Sex**		
Metabolite	**Coefficient**	**F**	**p**	**Coefficient**	**F**	**p**
tNAA	0.005	0.71	0.40	−0.17	1.33	0.25
NAA	0.004	0.87	0.35	−0.017	0.018	0.89
NAAG	−0.001	0.13	0.72	−0.17	6.63	**0.012**
tCho	0.006	14.24	**<0.001**	0.038	0.82	0.37
tCr	0.028	60.42	**<0.001**	0.07	0.53	0.47
mI	0.024	13.40	**<0.001**	0.008	0.002	0.96
Glx	0.011	0.99	0.32	0.31	1.10	0.30
Glu	0.003	0.23	0.63	0.14	0.56	0.46
Gln	0.006	1.84	0.18	0.19	2.30	0.13
GSH	0.002	1.00	0.32	0.045	0.95	0.33
sI	0.003	8.90	**0.004**	−0.026	1.14	0.29
PE	−0.002	0.25	0.62	−0.045	0.18	0.67
Lac	−0.001	0.24	0.62	−0.026	0.21	0.65
Asp	−0.002	0.70	0.41	−0.13	4.54	**0.036**
PCC						
	Age			**Sex**		
Metabolite	**Coefficient**	**F**	**p**	**Coefficient**	**F**	**p**
tNAA	0.004	0.63	0.43	−0.29	5.60	**0.020**
NAA	−0.001	0.073	0.79	−0.22	2.58	0.11
NAAG	0.007	9.10	**0.003**	−0.061	1.11	0.30
tCho	0.004	12.21	**0.001**	0.058	3.23	0.075
tCr	0.021	20.77	**<0.001**	0.005	0.002	0.97
mI	0.014	3.35	0.07	0.018	0.008	0.93
Glx	0.005	0.19	0.68	0.59	2.75	0.10
Glu	−0.002	0.067	0.80	0.18	0.71	0.40
Gln	0.011	3.26	0.074	0.36	5.21	**0.025**
GSH	0.002	1.23	0.27	−0.018	0.14	0.71
sI	0.002	3.85	0.053	−0.10	17.4	**<0.001**
PE	−0.004	0.79	0.38	−0.13	1.17	0.28
Lac	0.002	0.43	0.51	−0.23	5.19	**0.025**
Asp	0.001	0.052	0.82	−0.12	2.5	0.12

Table 4

Robust linear regressions and robust F-tests assessing separate contributions of sex, age, and the age*sex interaction to metabolite concentrations within each voxel. Coefficients represent robust regressions; F- and p-values are derived from robust F-tests. CSO results are presented first, followed by PCC results.

CSO									
Age				**Sex**			**Age*Sex Interaction**		
Metabolite	**Coefficient**	**F**	**p**	**Coefficient**	**F**	**p**	**Coefficient**	**F**	**p**
tNAA	0.005	0.41	0.52	−0.15	0.078	0.78	−0.001	0.003	0.96
NAA	0.004	0.37	0.55	−0.062	0.02	0.89	0.001	0.012	0.91
NAAG	<0.001	0.001	0.97	−0.091	0.176	0.68	−0.002	0.125	0.73
tCho	0.011	28.69	**<0.001**	0.48	12.34	**0.001**	−0.01	11.53	**0.001**
tCr	0.033	40.84	**<0.001**	0.50	2.13	0.15	−0.01	1.72	0.19
mI	0.035	14.41	**<0.001**	0.98	2.56	0.11	−0.023	2.867	0.094
Glx	0.011	0.49	0.49	0.30	0.083	0.77	<0.001	<0.001	0.99
Glu	0.004	0.18	0.68	0.20	0.097	0.76	−0.001	0.010	0.92
Gln	0.005	0.64	0.43	0.092	0.043	0.84	0.002	0.054	0.82
GSH	0.006	6.89	**0.010**	0.44	7.89	**0.006**	**−0.009**	**7.15**	**0.009**
sI	0.003	7.58	**0.007**	0.041	0.25	0.62	−0.002	0.79	0.38
PE	−0.001	0.027	0.87	0.062	0.028	0.87	−0.002	0.091	0.76
Lac	0.00	0.02	0.89	0.028	0.021	0.89	−0.001	0.088	0.77
Asp	−0.003	1.14	0.29	−0.26	1.50	0.22	0.003	0.41	0.53
PCC									
Age				**Sex**			**Age*Sex Interaction**		
Metabolite	**Coefficient**	**F**	**p**	**Coefficient**	**F**	**p**	**Coefficient**	**F**	**p**
tNAA	0.013	4.53	**0.036**	0.579	1.87	0.18	−0.02	4.76	**0.032**
NAA	0.008	1.24	0.27	0.649	1.98	0.16	−0.02	3.92	0.051
NAAG	0.007	4.88	0.030	−0.05	0.06	0.81	<0.001	0.003	0.95
tCho	0.008	21.63	**<0.001**	0.386	11.9	**0.001**	−0.007	9.17	**0.003**
tCr	0.034	29.96	**<0.001**	1.217	8.75	0.004	−0.028	9.59	**0.003**
mI	0.032	9.68	**0.002**	1.657	5.95	0.017	−0.037	6.48	**0.012**
Glx	0.012	0.44	0.51	1.156	0.89	0.35	−0.013	0.24	0.62

Glu	0.009	0.67	0.42	1.127	2.32	0.13	−0.021	1.81	0.18		
Gln	0.008	0.84	0.36	0.123	0.048	0.83	0.005	0.20	0.66		
GSH	0.004	3.17	0.078	0.186	1.29	0.26	−0.005	1.79	0.18		
sI	0.001	1.25	0.27	−0.142	2.59	0.11	0.001	0.21	0.65		
PE	−0.002	0.11	0.74	0.068	0.025	0.87	−0.005	0.24	0.63		
Lac	0.011	5.72	0.019	0.453	2.28	0.14	−0.016	6.04	**0.016**		
Asp	0.001	0.14	0.71	−0.048	0.033	0.86	−0.002	0.077	0.78		

Table 5

Robust linear regressions and robust F-tests assessing separate contributions of age, SNR, and FWHM linewidth to metabolite concentrations within each voxel. Coefficients represent robust regressions; F- and p-values are derived from robust F-tests. CSO results are presented first, followed by PCC results.

CSO									
Age				**SNR**			**FWHM**		
Metabolite	**Coefficient**	**F**	**p**	**Coefficient**	**F**	**p**	**Coefficient**	**F**	**P**
tNAA	0.006	1.20	0.28	0.018	29.32	**<0.001**	0.084	1.03	0.31
NAA	0.006	1.18	0.28	0.012	13.96	**<0.001**	0.039	0.27	0.61
NAAG	0.001	0.26	0.61	0.007	18.84	**<0.001**	0.011	0.086	0.77
tCho	0.007	15.14	**<0.001**	−0.004	14.68	**<0.001**	−0.061	5.68	**0.019**
tCr	0.028	37.52	**<0.001**	<0.001	0.014	0.907	0.002	0.001	0.98
mI	0.021	7.12	**0.009**	−0.01	4.75	**0.032**	−0.007	0.004	0.95
Glx	0.01	0.55	0.46	0.008	0.93	0.339	0.082	0.19	0.67
Glu	0.006	0.53	0.47	0.008	3.12	0.081	0.02	0.031	0.86
Gln	0.003	0.29	0.59	<0.001	0.018	0.892	0.071	0.71	0.40
GSH	0.001	0.46	0.50	<0.001	<0.001	0.983	0.005	0.023	0.88
sI	0.002	3.08	0.083	<0.001	0.49	0.487	0.019	1.56	0.22
PE	0.005	0.85	0.36	−0.006	4.44	**0.038**	−0.21	8.75	**0.004**
Lac	0.001	0.18	0.67	<0.001	0.011	0.916	−0.046	1.60	0.21
Asp	<0.001	<0.001	0.98	0.005	9.49	**0.003**	0.003	0.005	0.95
PCC									
Age				**SNR**			**FWHM**		
Metabolite	**Coefficient**	**F**	**p**	**Coefficient**	**F**	**p**	**Coefficient**	**F**	**p**
tNAA	0.009	2.53	0.115	0.006	3.18	0.078	−0.052	0.27	0.60
NAA	0.005	0.55	0.462	0.006	2.87	0.093	−0.093	0.68	0.41
NAAG	0.003	1.90	0.172	0.001	0.14	0.71	0.099	4.99	**0.028**
tCho	0.004	8.01	**0.006**	−0.001	1.98	0.16	−0.013	0.26	0.61
tCr	0.028	27.96	**<0.001**	−0.003	0.77	0.38	−0.27	7.76	**0.006**
mI	0.021	5.80	**0.018**	−0.009	3.02	0.085	−0.32	4.08	**0.046**
Glx	−0.002	0.024	0.876	−0.007	0.62	0.43	0.16	0.34	0.56
Glu	−0.003	0.072	0.789	−0.003	0.37	0.54	−0.024	0.02	0.89

Gln	0.004	0.34	0.564	−0.003	0.61	0.44	0.15		1.28	0.26	
GSH	0.004	2.88	0.093	−0.001	0.56	0.46	−0.056		2.34	0.13	
sI	0.003	5.18	**0.025**	<0.001	0.41	0.53	−0.032		2.05	0.16	
PE	0.007	1.97	0.164	−0.001	0.20	0.66	−0.32		12.39	**0.001**	
Lac	0.003	0.35	0.554	<0.001	<0.001	0.99	−0.018		0.048	0.83	
Asp	0.003	0.67	0.414	−0.002	1.041	0.31	−0.088		2.06	0.16	